MICROCHANNEL PLATES

Advances in Microchannel Plates and Photocathodes for Ultraviolet Photon Counting Detectors

INCOM

Bright Ideas in Fiber Optics

PH 508-909-2200 WWW.INCOMUSA.COM SALES@INCOMUSA.COM

Advances in Microchannel Plates and Photocathodes for Ultraviolet Photon Counting Detectors

O.H.W. Siegmund[a], K. Fujiwara[a], R. Hemphill[a], S.R. Jelinsky[a], J.B. McPhate[a], A.S. Tremsin[a], J.V. Vallerga[a], H.J. Frisch[b], J. Elam[c], A. Mane[c], D.C. Bennis[d], C.A. Craven[d], M.A. Deterando[d], J.R. Escolas[d], M.J. Minot[d], and J.M. Renaud[d]

[a]Experimental Astrophysics Group, Space Sciences Laboratory, 7 Gauss Way, University of California, Berkeley, CA 94720
[b]Enrico Fermi Institute, 5640 S. Ellis Ave. University of Chicago, Chicago, Il 60637
[c] Argonne National Laboratory, 9700 S. Cass Ave. Argonne, Il 60439
[d]Incom, Inc. 294 Southbridge Road, Charlton, MA 01507

ABSTRACT

A new method of fabricating microchannel plates has been investigated, employing microcapillary arrays of borosilicate glass that are deposited with resistive and secondary emissive layers using atomic layer deposition. Microchannel plates of this kind have been made in sizes from 33 mm to 200 mm, with pore sizes of 40 μm and 20 μm, pore length to diameter ratios of 60:1, bias angles of 8°, and open areas from 60% to 83%. Tests with single MCPs and MCP pairs have been done and show good imaging quality, gain comparable to conventional MCPs, low background rates (~ 0.085 events sec^{-1} cm^{-2}), fast pulse response, and good ageing characteristics. The quantum efficiency for bare and alkali halide coated MCPs is similar to conventional MCPs, and we have also been able to deposit opaque GaN(Mg) cathodes directly onto these MCPs.

Keywords: Microchannel Plates, Imaging, Photon Counting, Photocathodes.

1. INTRODUCTION

Microchannel plates (MCPs) have been used as electron multipliers for many decades and are particularly useful in imaging photon counting detector schemes[1-8] for applications in a wide variety of fields. MCPs can be used in open face detectors and in sealed tube sensors at high vacuum with photocathodes [9] for detection of charged particles, neutrons and photons in both analog and event counting modes. Sensors with MCPs have beeen constructed with spatial resolution as small as 5 μm, event time recording down to ~ 10 ps, with background rates of < 0.03 events cm^{-2} sec^{-1}, gain up to 10^8, lifetimes of up to 10's of Coulombs cm^{-2}, quantum efficiency of >60%, and formats of up to 150 mm. The basic methodology for fabrication of MCPs[8] has changed very little for many years. Glass filled glass tubes (proprietary lead glass compositions) are made and drawn down to small sizes in a furnace, cut, stacked and fused into hexagonal bundles, which are sometimes drawn down again, and stacked together then fused to form a block. This is cut into slices, at a set bias angle, which are then polished. The core glass is subsequently etched out, and the clad glass is reduced in a hydrogen furnace to produce surfaces with high secondary emission coefficient and to make the MCP resistive (MΩ). Lastly the top and bottom surfaces are coated with a metal layer (usually NiCr) to allow a high voltage to be applied across the MCP. Although this process is highly successful it can also lead to problems in some performance parameters[9,10] and can be quite expensive for some custom and large MCP configurations. Alternate solutions for fabrication of MCPs have been investigated for many years, including silicon[11] based MCPs and anodic alumina[12]

MCPs. These have had limited success and still have considerable issues to resolve before they can be considered viable alternatives. Under a DOE funded program initiated by a collaboration of Universities, National Laboratories and Industries to develop a Large Area Picosecond Detector[13] another method for construction of MCPs has been investigated. Microcapillary arrays can be constructed beginning with inexpensive hollow borosilicate tubes. The fabrication method is similar to that for conventional MCPs except that there is no etching of core glass, since there is no glass filling. The second fundamental change is the deposition of a resistive layer and a secondary emissive layer over the entire microcapillary array using an atomic layer deposition (ALD) process[14] that has recently become more generally available. The contact electrodes can be applied either before, or after the ALD processes, or both. This method for making MCPs has the advantage that each step is essentially independent and can be tailored to suit each operational parameter required. Specific properties of ALD borosilicate MCPs include a high glass softening temperature (>700 °C) which may allow a range of previously unfeasible processes to be accomplished with these as substrates. The fabrication method and materials are inherently cleaner than the wet chemistry used for conventional MCPs suggesting that potential contamination, and outgassing may be significantly lower. This would have a direct effect on MCP detector lifetimes in sealed tube devices, and in reduction of contamination of photocathodes. The absence of lead in the glass reduces the gamma ray cross section and thus the background in high gamma ray flux environments. The low radioactivity glass composition suggests that the intrinsic MCP background will be lower than conventional MCPs[15]. We have instituted a program of assessment of the ALD borosilicate substrate MCP scheme, and have made an extensive tests to evaluate its potential.

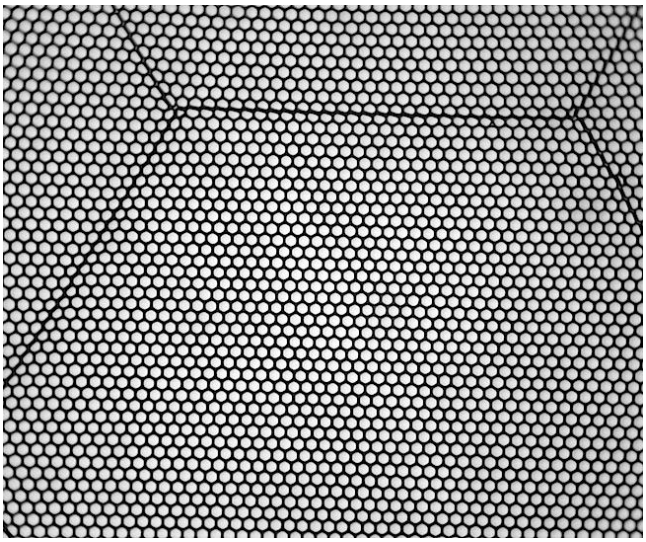

Figure 1. 200 mm square.borosilicate micro-capillary substrate, magnified section, 20 µm pores, 65% open area.

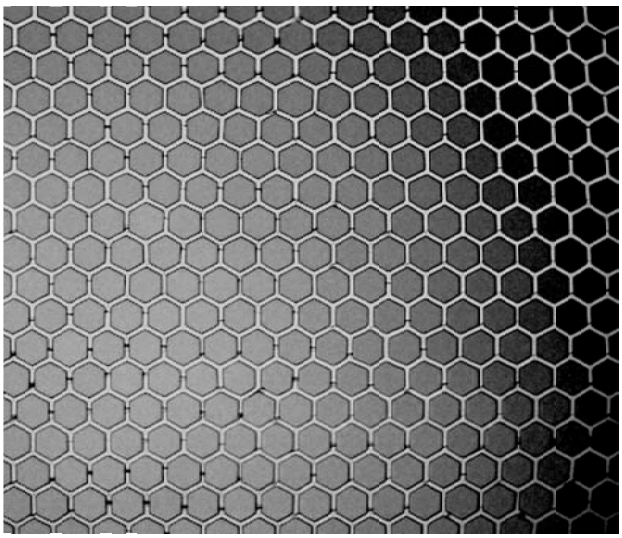

Figure 2. 33 mm diameter. borosilicate micro-capillary substrate, substrate, magnified section, 40 µm pores with 83% open area.

2. BOROSILICATE SUBSTRATE, ATOMIC LAYER FUNCTIONALIZED MCPS

We have fabricated borosilicate microcapillary substrates (at INCOM Inc.) for use as the starting point for MCPs. The pore sizes are 40 µm and 20 µm, with pore length to diameter (L/d) ratio of 60:1 and a bias angle cut of 8° to normal. The substrate sizes range from 33 mm to 200 mm, and the open area fraction varies from 65% to 83%. Early materials suffered from various defects but there have been rapid improvements and good substrates (Figs. 1, 2) are now routinely available.

ALD functionalization was performed at Arradiance Inc. and at Argonne National Laboratory (ANL). The 33 mm substrate size was adopted as a test article evaluation standard, and most of the tests to date have been done with this size. The ALD functionalization can produce MCPs with resistances over a wide range, from a few MΩ up to GΩ although values in the range 30 to 500 MΩ are most useful. A number of different, proprietary, resistive and secondary emissive layers have been applied and evaluated. Most of the tests reported here have been accomplished with the conductive electrode applied as the last process.

Figure 3. 33 mm diameter. borosilicate substrate MCP with ALD layers and NiCr electrodes, 20 µm pores, 65% open area.

Figure 4. 33 mm borosilicate substrate MCP with ALD and NiCr electrodes, 20 µm pores, 65% open area. Backlit photo.

3. 33 MM BOROSILICATE SUBSTRATE, ATOMIC LAYER MCP PERFORMANCE

Extensive testing of ALD functionalized borosilicate MCPs has been done to assess their performance, and to assist with the optimization of the construction and functionalization processes. The majority of these tests have been done with the 33 mm format devices as this is a standard size for MCPs and we can accommodate them in detector devices that have been designed for this purpose. Two types of detector have been used for these tests, both of which are “open face” to allow direct stimulation of the MCPs with ultraviolet light. One detector is a fairly simple housing that accommodates one, or two MCPs, and has a < 1 mm gap with a phosphor screen readout. The phosphor is biased at ~+ 3 kV with respect to the MCP output face so that visible images of the MCP signal can be recorded. The phosphor can also be biased at ~ +45 V, to allow connection of a picoammeter to measure the output current. The front of the MCP to be tested is biased negative, and can be illuminated with a 184 nm UV source through a sapphire window in the vacuum tank. Alternately we can put a second MCP, above the test MCP, and use the first MCP as an electron source for the testing. The second type of detector accommodates two MCPs, and has a ~ 5 mm gap with a cross delay line readout, and associated electronics for photon position and time determination. Both detector types permit pairs of MCPs to be stacked with a gap between them and accommodate a potential to be applied across that gap. There are also two kinds of each detector, one type that is constructed of only ceramic and metal materials that can be baked to 400 °C, and

another type using thermoplastics that can only be baked to ~ 150°C. A wide range of tests of ALD functionalized borosilicate MCPs have been undertaken with these detectors, as outlined below. Evaluations include the spatial resolution, image distortion, uniform illumination fixed pattern noise, gain and gain uniformity, pulse amplitude distribution, background event rates and spatial distribution, event speed and shape, quantum efficiency, and stability of performance when subjected to preconditioning processes[16] such as vacuum bakeout and extended "burn-in".

3.1. MCP Gain, and Imaging Characteristics

For the initial tests the phosphor readout detector was used. This allows a quick assessment of the imaging quality in "DC" current gain mode, and a rapid evaluation of the single MCP gain. The gain v.s. voltage characteristic for two individual 20 µm pore, 60:1 L/d, 8 degree pore bias MCPs illuminated with low energy electrons is shown in Fig. 5. Over a wide range of gains the logarithmic gain characteristic is maintained, only showing some indications of gain saturation at gains above 10^4, in common with conventional MCPs [17]. Many more gain assessments have been made[18] and all are in close accord with conventional MCP characteristics. The imaging quality depends on a number of issues including the fabrication of the borosilicate substrates and the ALD functionalizations. Initial materials had a number of issues[19] but were still quite useful. Rapid progress has been made and the quality of substrates has improved dramatically. Images taken with the phosphor screen (Fig. 6) show a few defects and a very sharp well defined multifiber modulation pattern that is characteristic of many conventional MCPs.

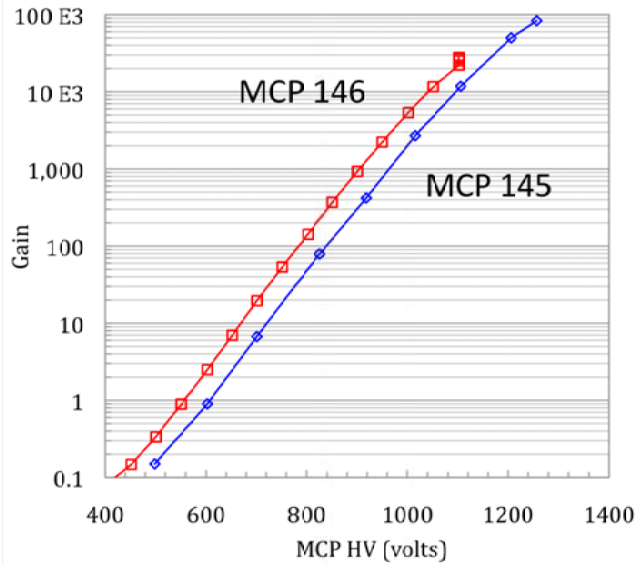

Figure 5. Gain as a function of applied voltage for single ALD borosilicate MCPs with electron input. 20 µm pores, 65% open area, 60:1 L/d, 8 degree pore bias.

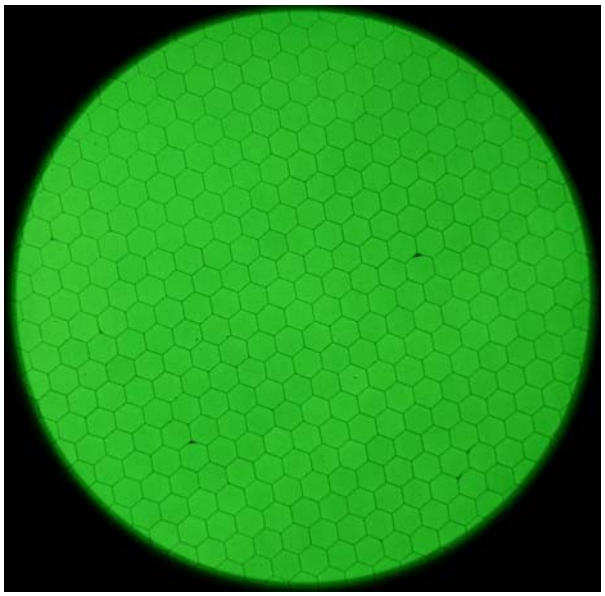

Figure 6. Image for 185 nm illumination, of a 33 mm ALD borosilicate MCP using a phosphor screen readout. 20 µm pores, 65% open area, 60:1 L/d, 8° pore bias. 1100V MCP.

The level of the hexagonal modulation of the image is indicative of the amount of physical distortion of the pores at the boundary. As seen in Fig. 1, the distortions are mostly restricted to only one pore either side of the boundary, and this correlates well with the sharply defined modulations seen in Fig. 6. The general uniformity of the intensity of the image indicates the overall uniformity

of the size and shape of the pores over the entire substrate. Better diagnostics are available however in the pulse counting mode with a pair of MCPs.

A significant number of MCP pairs have been tested using the cross delay line detector. Gain v.s. voltage curves can be obtained over a wide range (Fig. 7) from event pulse counting at the higher gains to analog gain operation at the lower gain. The bump in the gain curve in Fig. 7 is at the point where our gain measurements transition from event pulse counting to analog operation, below ~ 3 x 10^4 gain. The overall gain curve is consistent with observations of conventional MCPs [17] and shows the gain saturation that occurs at high gain, with the accompanying tightening of the event pulse height distribution (Fig. 8). The pulse height distributions are not as narrow as the three-MCP stacks that we often use, but are within the normal range for conventional MCP pairs of a similar physical specification. Adding a gap between the two MCPs and applying a bias on this we can increase the overall gain to over 10^7.

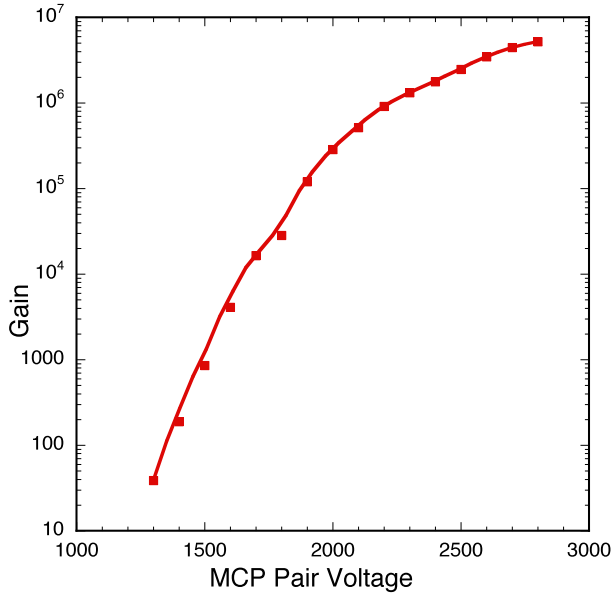

Figure 7. Gain as a function of voltage for a 33mm ALD back to back MCP pair, 20µm pore, 60:1 L/d, 8 degree bias.

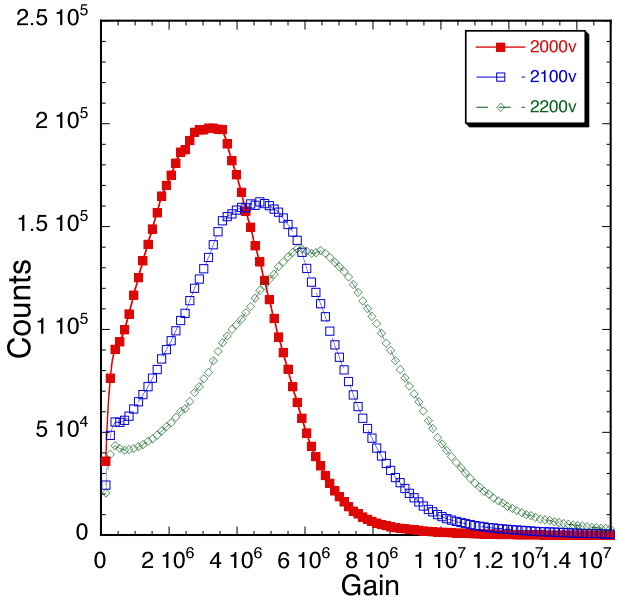

Figure 8. Pulse height amplitude distributions for a 33mm ALD back to back MCP pair, 40µm pore, 60:1 L/d, 8 degree bias.

The imaging performance of the MCP pairs has been evaluated with the cross delay line detector using full flood UV illumination (Fig. 9). The fixed pattern noise seen in Fig. 9 is derived from several effects. The edge distortions are due to reflections from the MCP clamping hardware and field fringing due to the MCP support flange. The remaining features are a few MCP defects, and the hexagonal modulation due to the packing structure of the MCPs. There are two hexagonal patterns, the sharp, dark pattern is the top MCP and a fainter pattern is due to the lower MCP. All these features can be removed by dividing any dataset by a calibration flat field, since the pattern is stable and consistent. There is a also a very faint bright band across the image which is due to a band several multifibers wide where the MCP pores are slightly larger. This can also be seen in the back-lit image in Fig. 4.

Since the gain of each event is recorded it is possible to plot an "image" of the average gain of the MCP pair (Fig. 10). This shows that the top MCP hexagonal modulation boundaries have lower gain at these interfaces, as one might expect from the pore distortions. There are also a few patches with slightly low gain which can also faintly be seen on the "flux" image (Fig. 9). Otherwise the

gain is very constant, with multifiber to multifiber differences of only a few percent. Overall, the results are similar to many conventional MCPs [10] and support the method of ALD functionalization of borosilicate microcapillary arrays for construction of large area microchannel plates.

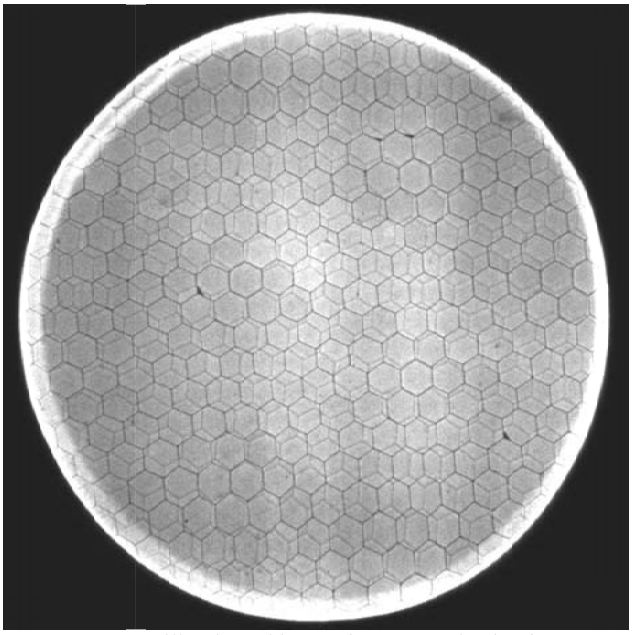

Figure 9. 184 nm illuminated image for a gapped pair of 20 µm pore 60:1 L/d, 8 degree bias, ALD MCPs. 0.7 mm gap with 300 V bias. Gain ~ 8 x 10^6 with ~1000 V on each MCP. 26 mm area.

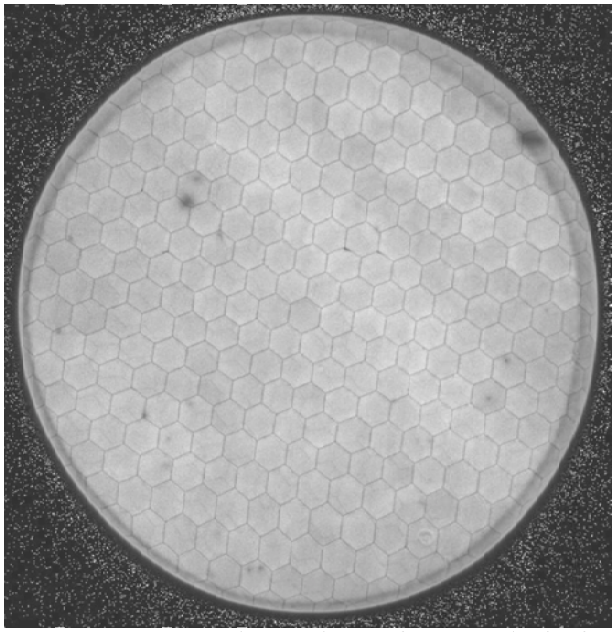

Figure 10. Average gain map "image" for a gapped pair of 20 µm pore 60:1 L/d, 8 degree bias, ALD MCPs. 0.7 mm gap with 300 V bias. Gain ~ 8 x 10^6 with ~1000 V on each MCP.

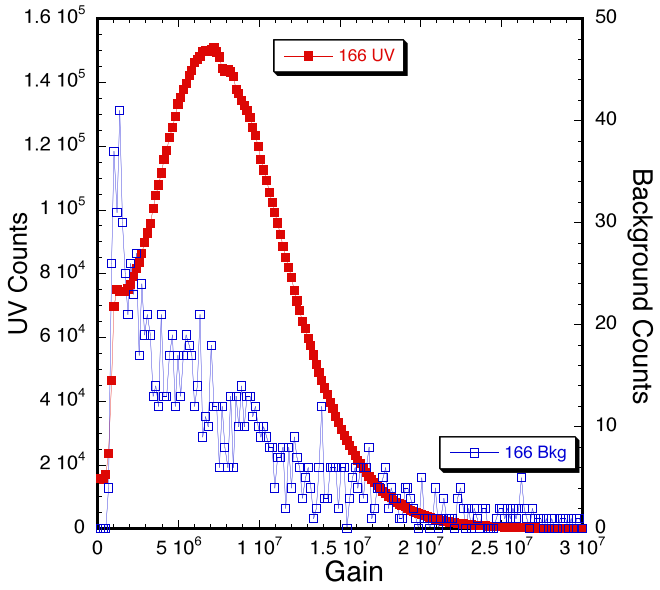

Figure 11. 184 nm UV and background pulse amplitude distributions for a gapped pair of 20 µm pore 60:1 L/d, 8 degree bias, ALD MCPs. 0.7 mm gap with 300 V bias. Gain ~ 7 x 10^6.

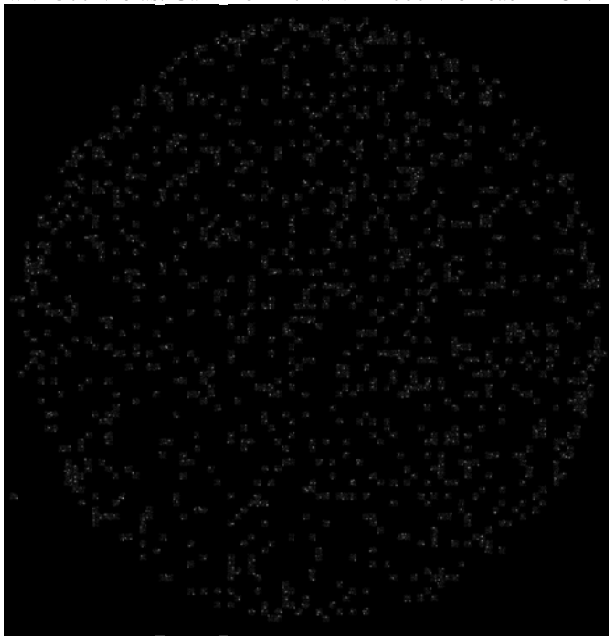

Figure 12. Background event "image" for a gapped pair of 20 µm pore 60:1 L/d, 8 degree bias, ALD MCPs. 0.7 mm gap with 300 V bias. Gain ~ 7 x 10^6 with ~1000 V on each MCP. ~0.085 events cm^{-2} sec^{-1} in 3000 sec.

3.2. *MCP Background Characteristics*

The background rate of many pairs of ALD functionalized borosilicate MCPs have been measured in a photon counting, imaging detector with a cross delay line readout. In some cases there are "warm spots" corresponding to debris on the MCPs, but in most cases the background rate and spatial distribution are very consistent. We find that the amplitude distribution of background events has a exponentially declining shape (Fig. 11), commensurate with these events being generated uniformly through the depth of the MCPs. Spatial distribution of background events is also uniform (Fig. 12) suggesting that the background is a phenomenon causing events homogeneously throughout the bulk of these MCPs. The typical event rate is of the order ~ 0.085 events sec^{-1} cm^{-2}, which is substantially lower than conventional MCPs in this configuration. The ALD borosilicate MCP composition is quite different than conventional MCPs. There is no lead in the glass, and the alkali content (and their radioactive isotopes) is much lower. The comparable background rate for conventional MCP glasses is ~0.25 events sec^{-1} cm^{-2} using potassium-lead glasses, but can be as low as 0.03 events sec^{-1} cm^{-2} for "radioactive free" MCP glass[15] (determined by the cosmic ray flux – Muon detection rate). Given its low gamma ray cross section, and its low background rate, borosilicate glass ALD functionalized MCPs are an attractive choice for low background applications.

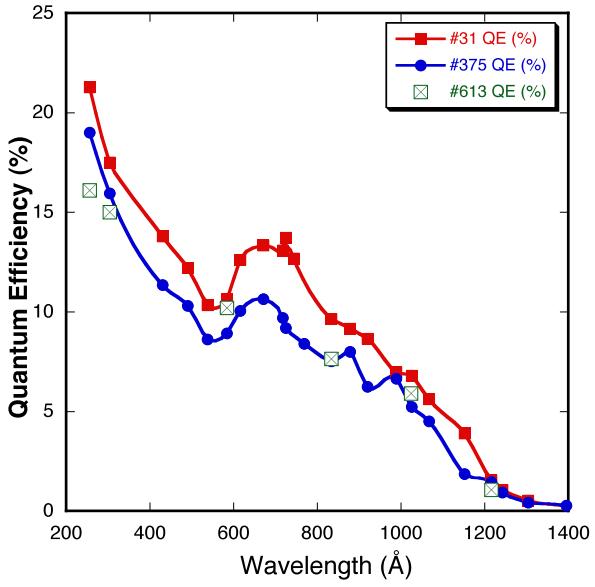

Figure 13. UV Quantum detection efficiency measurements for pairs of 20 µm pore (375 & 613, 65% open area) and 40 µm pore (31, 83% open area) 60:1 L/d, 8 degree bias, ALD MCPs.. Gain ~ 5 x 10^6. Input angle ~15 ° to pore axis.

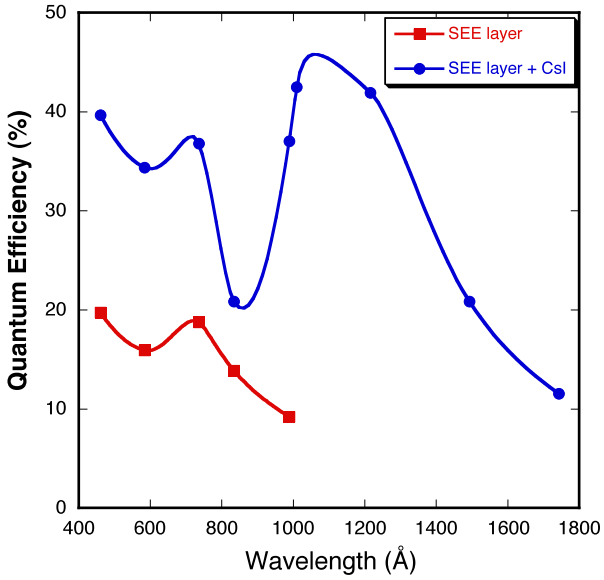

Figure 14. UV Quantum detection efficiency measurements for a pair of 12 µm pore conventional MCPs, 80:1 L/d, 12° bias, gain ~ 5 x 10^6. ALD SEE layer was deposited onto these, later a CsI photocathode was added. UV input angle ~15 ° to pore axis.

3.3. *MCP Event Detection Efficiency and Photocathode Compatibility*

The quantum detection efficiency of several ALD MCPs was measured in the ultraviolet regime. The ALD MCPs selected had 20 µm or 40 µm pores, 60:1 L/d, 8 degree bias, and were tested as resistance matched pairs. All the ALD MCPs had NiCr electrode layers deposited on their surfaces after the ALD depositions. Since this is the same surface used on conventional MCPs we expect that the QDE will be similar to those we achieve with conventional MCPs [9]. In Fig. 13 we show the measurements for ALD MCPs, and these are in general accord with our expectations. Of note is the

QDE drop at ~600 Å which is a signature of the onset of two photoelectron production (~2 x the effective photoelectric threshold energy). This is more prominent than for conventional MCPs and may be indicative of the higher secondary emission coefficient of the secondary electron emissive ALD layer used on these MCPs. The 40 µm pore ALD MCPs also seem to have higher QDE than the 20 µm pore ALD MCPs. This is a result of the open area ratio for the 40 µm ALD MCPs being ~83% rather than 65% for the 20 µm pore ALD MCPs. Another potential consequence is a corresponding increase in the electron and ion detection efficiencies, although this has yet to be confirmed by doing appropriate measurements.

Tests have also been done to assess the efficiency of the secondary electron emissive ALD layer applied to the MCPs. We have measured the UV QDE of conventional MCPs coated with a secondary electron emissive ALD layer (Fig. 14). The QDE is similar to a bare MCP, but the QDE is enhanced at ~700 Å, so at ~2 x the effective photoelectric threshold energy. Coating the MCP with a CsI photocathode on top of the secondary electron emissive ALD layer we achieve a standard CsI/MCP QDE response [9]. A biased QDE enhancement grid to collect web photoelectrons was implemented for these measurements.

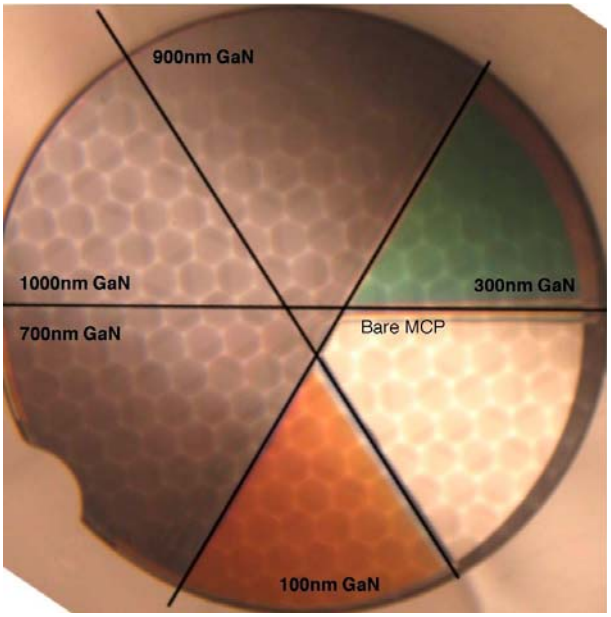

Figure 15. GaN deposited in different thickness zones on a 20 µm pore 60:1 L/d, 8 degree bias, ALD functionalized borosilicate substrate MCP. GaN(Mg) deposited by molecular beam epitaxy.

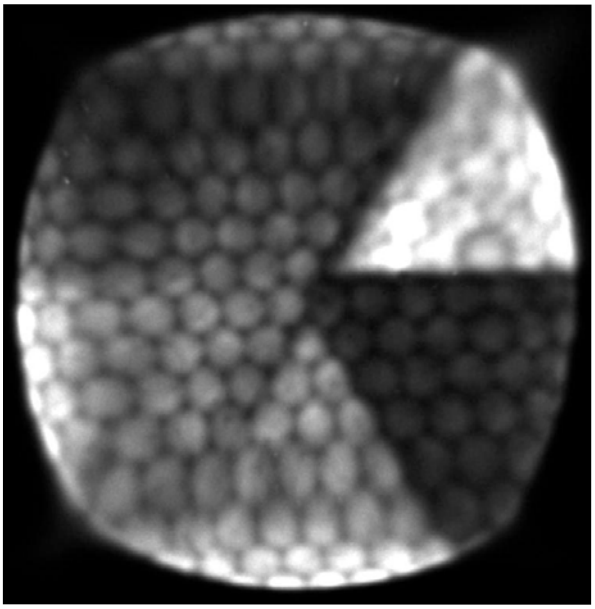

Figure 16. UV (184 nm) illuminated image obtained with a pair of ALD MCPs, with the GaN coated MCP in Fig. 15 on top. Gain ~ 6 x 10^6 with ~1000 V on each MCP.

We have also deposited GaN(Mg) photocathodes (SVT Inc. by MBE) onto ALD-MCPs (Fig. 15) with various thicknesses in zones on a single MCP. Substrate conditions, P dopant levels and concentration grading play significant roles[12] in the QE achieved. GaN layers are not optimally deposited onto the NiCr surface, but we have previously measured conventional MCPs coated with MBE deposited GaN(Mg) with some success[12]. Using a pair of ALD functionalized borosilicate MCPs in a photon counting, imaging detector with a cross delay line readout we have examined the initial photo-response of the as-deposited GaN layers (Fig. 16). Without reduction of the electron affinity by cleaning and Cs deposition steps, the overall quantum efficiency is low. This will be accomplished next, but even without this step is clear that the GaN has a considerable photo-

response enhancement effect. The 300nm thick GaN coated area has ~8 x the response of the uncoated MCP area, but thicker GaN areas have progressively lower response. The 100 nm thick zone has similar response to the 700 nm thick zone. The overall response is a function of the photoelectron mean free path, the surface escape probability and the photon absorption depth. The optimal thickness will change as these quantities are manipulated by surface cleaning and Cs activation steps. More studies are currently underway to perform the surface cleaning and Cs activation steps and determine the best thickness.

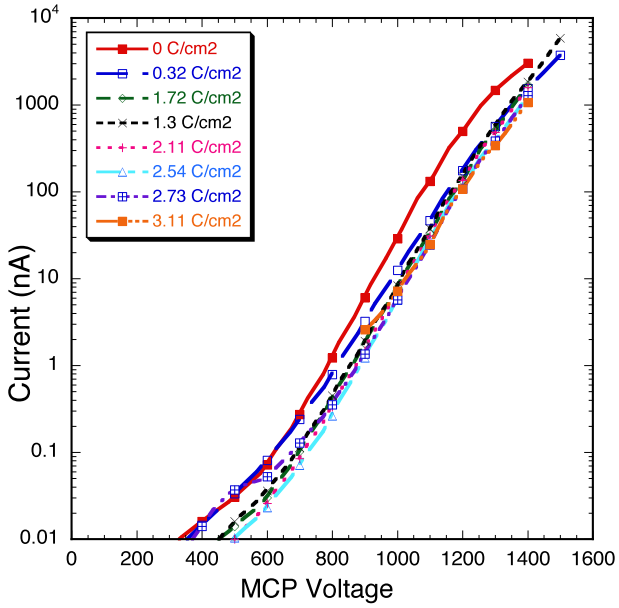

Figure 17. Gain curves for a single borosilicate-ALD MCP with 20 µm pores, 60:1 L/d, 8 degree bias, as a function of extracted charge during UV burn-in (~0.5 µA cm^{-2}), (after a 150°C bakeout).

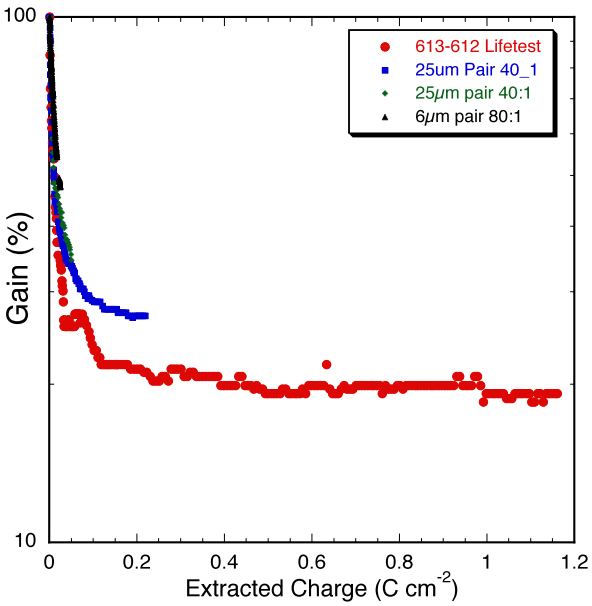

Figure 18. Gain for a borosilicate-ALD MCP pair (613-612) with 20 µm pore, 60:1 L/d, 8 degree bias, as a function of extracted charge during UV burn-in (~0.5 µA cm^{-2}) (after a 350°C bakeout), compared to conventional MCPs.

3.4. MCP Preconditioning and Lifetime Characteristics

One of the most important issues pertaining to MCPs is their overall lifetime behavior. Considerable effort[16] has been put into the manufacture and preparation of MCPs to improve their stability and longevity. After MCP fabrication the preparation for use in high vacuum devices often entails preconditioning steps; a vacuum bake-out to remove adsorbed gasses and contaminants, and a "Burn In" to continue this process and stabilize the long term gain behavior. We have examined the behavior of ALD borosilicate MCPs when subjected to these preconditioning steps to assess their performance compared to conventional MCPs. Two cases were examined. A single ALD borosilicate MCP in a detector with a phosphor screen readout, and a resistance matched pair of ALD borosilicate MCPs in a detector with a photon counting, imaging cross delay line readout. The single MCP was subjected to a 150 °C vacuum (< 10^{-5} Torr) bake for 48 hours predominately to remove water vapor, and then illuminated with a high flux of 184 nm UV and operated at an output current of ~0.5 µA cm^{-2} to "burn in" the gain to achieve stabilization. Periodically the gain v.s. applied voltage curves were remeasured (Fig. 17, output current for a fixed input flux) to assess the progress of the burn-in. After the first 0.32 C cm^{-2} of charge extraction the gain curves are essentially stabilized, which is similar to the trends seen for conventional MCPs.

The MCP pair was subjected to a 350 °C vacuum (< 10^{-5} Torr) bake for 20 hours and monitored with a residual gas analyzer. The gasses released were predominantly those found in air along with water vapor and hydrogen. Subsequently a "burn-in" was done with a high flux of 184 nm UV at output currents up to ~0.5 μA cm^{-2} at relatively low overall gain (~ 10^4). The relative gain change was continuously monitored (Fig. 18), accounting for the periodic adjustments of gain to maintain the output current level. After the first 0.2 C cm^{-2} of charge extraction the gain stabilizes. This can be compared to results with conventional MCPs (Fig. 18). The initial gain drop is associated with considerable gas evolution from the surfaces of the MCP pores. The gain stabilization is qualitatively similar to conventional MCPs, however more detailed study is needed to establish the specific gas evolution rate after the burn in process, as this is a critical factor in determination of the lifetime of photocathodes in sealed tube configurations.

3.5. MCP Event Time Signal Characteristics

Some applications require that the individual event times to be determined (Cherenkov imaging, biological fluorescence lifetime imaging, LIDAR, time resolved astronomy, time of flight imaging mass spectroscopy etc). We have time tagged single photon events with various MCP detector systems and achieved timing jitter [2] of about 100 ps FWHM for MCP pulses < 2ns in width using conventional MCPs. The timing characteristics of ALD borosilicate MCPs[18] has been measured (Fig. 19) and is found to be in general accord with conventional MCPs. The ~1 ns pulse width seen for a pair of 20 μm pore MCPs (0.7 mm gap with 150 V bias) is significantly affected by the 1 GHz analog oscilloscope bandwidth (130 ps risetime preamplifier also used). Models and measurements undertaken at Argonne National Laboratory[18] indicate that the fast pulse response characteristics are better than this, and we will subsequently make measurements with higher bandwidth electronics to evaluate it.

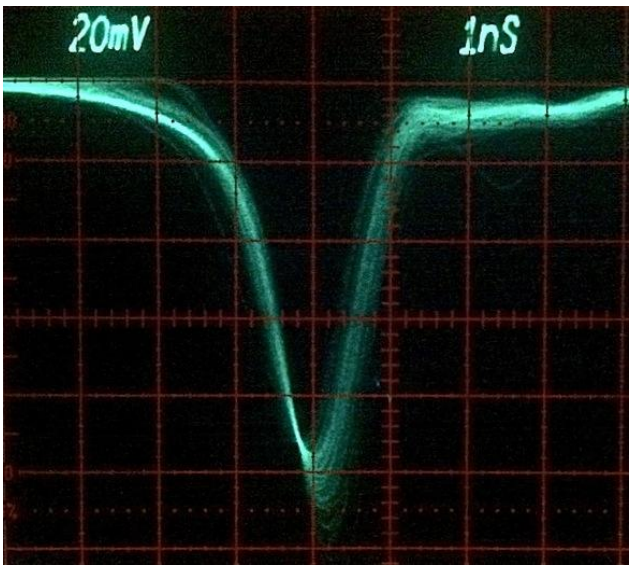

Figure 19. MCP output pulses for a gapped pair of 20 μm pore 60:1 L/d, 8 degree bias, ALD MCPs. 0.7 mm gap with 150 V bias. 184 nm illumination, trigger threshold set high to show pulse shape. Gain ~ 8 x 10^6 with ~1100 V applied to each MCP.

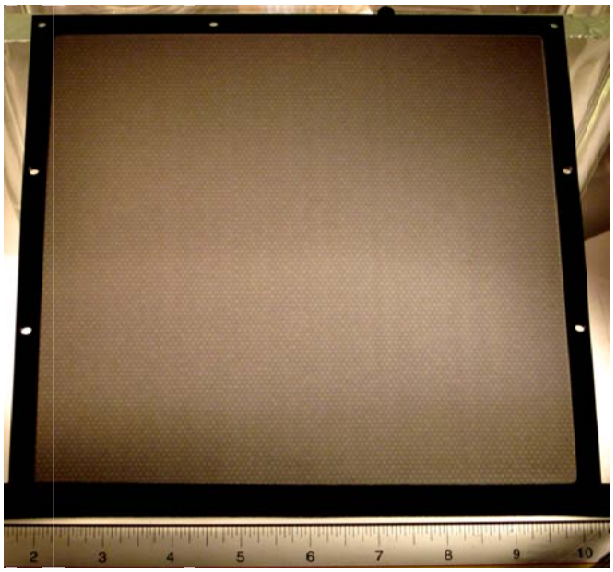

Figure 20. Back illuminated photo of a 200 x 200 mm ALD MCP with 20 mm pore borosilicate substrate. Contrast enhanced to show the MCP multi-fibers. Also see Fig. 1.

3.6. Progress with 20 cm Borosilicate Substrate, Atomic Layer MCPs

20 x 20 cm borosilicate substrates in 20 µm and 40 µm pore material have been ALD functionalized (Fig. 20). These currently have good overall multi-fiber packing structure and low pore distortions (Fig. 1). Back-illuminated examination (Fig. 20) confirms that the overall uniformity is also quite good. One of the first articles has been tested under vacuum to determine the gain and stability of operation of this size MCP. The resistance of this MCP, which is already quite small, drops as the applied voltage is increased. This is a result of the heating of the MCP and the negative coefficient of resistance v.s. temperature of the ALD resistive layer. The power dissipation is sufficiently high that prolonged operation for this MCP is likely to be problematic. The ALD technique, however, allows a wide range of possible resistance values to be achieved, so subsequent samples can be adjusted to higher values. Nevertheless, using UV illumination we were able to observe normal MCP gain behavior (Fig. 22) over a similar range of applied voltages used for the 33 mm sample MCPs (Figs. 5, 17). Considerable future work is planned to optimize and characterize the 20 cm ALD borosilicate MCPs, but the initial tests are a positive sign that this technique has promise for large area MCP implementation.

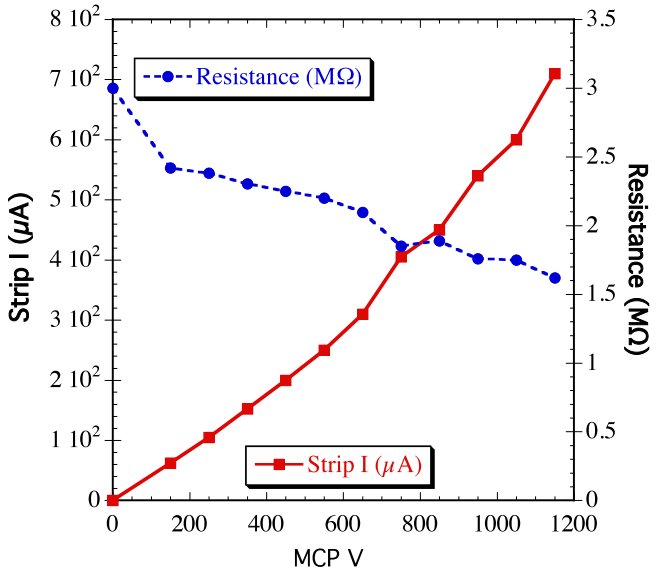

Figure 21. Resistance and MCP bias (strip) current for a 200 mm square ALD MCP with 20 mm pore borosilicate substrate, 60:1 L/d, 8 degree bias, 65% open area, 184 nm UV illumination.

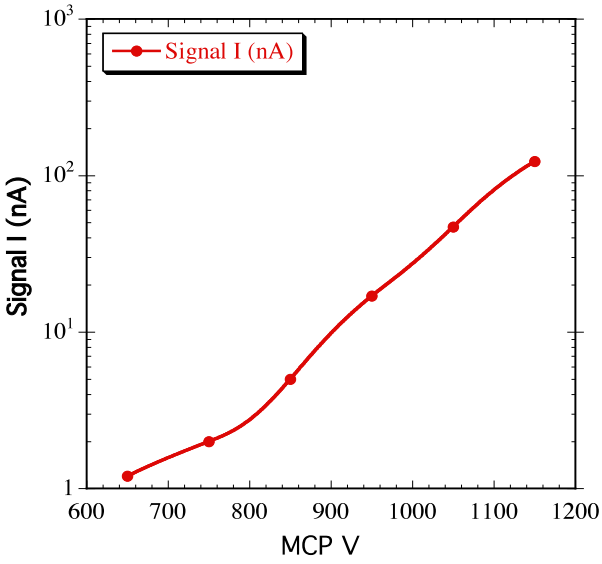

Figure 22. Output signal v.s. voltage for a 200 mm square ALD MCP with 20 mm pore borosilicate substrate, 60:1 L/d, 8 degree bias, 65% open area, 184 nm UV illumination.

ki

ACKNOWLEDGEMENTS

We wish to thank J. Hull, J. Tedesco, R. Wagner, A. Dabiran at SVT Inc. and Arradiance. Inc. for their contributions to this work. This work was supported by under DOE contract DE-AC02-06CH11357, and NASA grant NNX11AD54G.

REFERENCES

1. O.H.W. Siegmund, J.V. Vallerga, B. Welsh, J. McPhate, A. Tremsin, "High speed optical imaging photon counting microchannel plate detectors for astronomical and space sensing applications", Proceedings of the Advanced Maui Optical and Space Surveillance Technologies Conference. p. 90. (2009),

2. O. Siegmund, J. Vallerga, P. Jelinsky, X. Michalet, and S. Weiss, "Cross Delay Line Detectors for High Time Resolution Astronomical Polarimetry and Biological Fluorescence Imaging", Proc. IEEE Nuclear Science Symposium, ISBN: 0-7803-9222-1, pp. 448-452, 2005.
3. A.S. Tremsin, G.V. Lebedev, O.H.W. Siegmund, J.V. Vallerga, J.B. McPhate, Z. Hussain, "High resolution detection system for time of flight electron spectrometry", Nucl. Instr. Meth. A582 pp.172-174, (2007).
4. O.H.W. Siegmund , B.Y. Welsh, J.V. Vallerga, A.S. Tremsin, J.B. McPhate, "High-performance microchannel plate imaging photon counters for spaceborne sensing", Proc. SPIE **6220**, (2006).
5. A.S. Tremsin, O.H.W. Siegmund, J.V. Vallerga, J. Hull, "Cross Strip Readouts for Photon Counting Detectors with High Spatial and Temporal Resolution", IEEE Trans. Nucl. Sci.. 51 (N4) pp.1707-1711 (2004).
6. O. H. W. Siegmund, P. Jelinsky, S. Jelinsky, J. Stock, J. Hull, D. Doliber, J. Zaninovich, A. S. Tremsin and K. Kromer, "High resolution cross delay line detectors for the GALEX mission", *Proc. SPIE* **3765**, pp.429-440 (1999).
7. O.H.W. Siegmund, Methods of vacuum ultraviolet physics, Chapter III, 2nd edition, ed's J.A.R. Samson and D.L. Ederer, Academic Press, (1998).
8. M. Lampton, The microchannel image intensifier, Scientific American, **245**, 62-71, (1981).
9. O.H.W. Siegmund, John Vallerga, Anton Tremsin, "Characterizations of microchannel plate quantum efficiency", *Proc.* SPIE. **5898**, 58980H, (2005).
10. O.H.W. Siegmund, J. Vallerga, A. Tremsin, J. McPhate, "Microchannel plates: recent advances in performance", Proc. SPIE **6686**, , 66860W (2007).
11. O.H.W. Siegmund Advances in microchannel plate detectors for UV/visible Astronomy, Proc. SPIE Vol. 4854, pp 181-190, (2003)
12. O.H.W. Siegmund, Tremsin, Anton S., Vallerga, John V., McPhate, Jason B., Hull, Jeffrey S., Malloy, James, Dabiran, Amir M. "Gallium nitride photocathode development for imaging detectors" Proc. SPIE, Vol. 7021, p.40, (2008)
13. H.J. Frisch, "The development of large-area detectors with space and time resolution", Advances in Neutrino Technology workshop, (2009).
14. M. Ritala and M. Leskelä. Nanotechnology, **10:1**, 19. (1999)
15. O.H.W. Siegmund, M.A. Gummin, J. Stock and D. Marsh, "Microchannel plate imaging detectors for the ultraviolet", ESA symposium on detectors, **ESA SP-356**, (1992).
16. O.H.W. Siegmund, "Preconditioning of microchannel plate stacks," *Proc. SPIE*, **1072**, 111-118 (1989).
17. J.L. Wisa, "Microchannel plate detectors", Nucl. Instr. Meth. 162 pp.587-601, (1979)
18. M. Wetstein, "Development of sub-nanosecond, high gain structures for time of flight ring imaging in large area detectors",Nucl. Instr. Meth. **639(1)**, pp148-150, (2011)
19. O.H.W. Siegmund, J.B. McPhate[a], J.V. Vallerga[a], A.S. Tremsin[a], S.R. Jelinsky[a], H.J. Frisch, "Novel large format sealed tube microchannel plate detectors for Cherenkov timing and imaging", Nucl. Instr. Meth. **639(1)**, pp165-168, (2011)

Incom Inc.
294 Southbridge Road
Charlton, MA 01507 USA
P: 508-909-2200
sales@incomusa.com
www.incomusa.com